International Journal of Naval Architecture and Ocean Engineering 10 (2018) 596–608

Contents lists available at ScienceDirect

International Journal of Naval Architecture and Ocean Engineering

journal homepage: http://www.journals.elsevier.com/international-journal-of-naval-architecture-and-ocean-engineering/

Uncertainty assessment for a towed underwater stereo PIV system by uniform flow measurement

Bum Woo Han [a], Jeonghwa Seo [b, *], Seung Jae Lee [b], Dong Myung Seol [c], Shin Hyung Rhee [b, d]

[a] Hyundai Maritime Research Institute, Hyundai Heavy Industries, Co. Ltd., Ulsan, Republic of Korea
[b] Research Institute of Marine Systems Engineering, Seoul National University, 1 Gwanak-ro, Gwanak-gu, Seoul, Republic of Korea
[c] Defense Acquisition Program Administration, Seoul, Republic of Korea
[d] Dept. of Naval Architecture and Ocean Engineering, Seoul National University, Seoul, Republic of Korea

ARTICLE INFO

Article history:
Received 26 December 2015
Received in revised form
1 November 2017
Accepted 24 November 2017
Available online 30 December 2017

Keywords:
Stereoscopic particle image velocimetry
Towing tank experiment
Test uncertainty

ABSTRACT

The present study aims to assess test uncertainty assessment method of nominal wake field measurement by a Stereoscopic Particle Image Velocimetry (SPIV) system in a towing tank. The systematic uncertainty of the SPIV system was estimated from repeated uniform flow measurements. In the uniform flow measurement case, time interval between image frames and uniform flow speed were varied to examine the effects of particle displacement and flow around the SPIV system on the systematic standard uncertainty. The random standard uncertainty was assessed by repeating nominal wake field measurements and the estimated random standard uncertainty was compared with that of laser Doppler velocimetry. The test uncertainty assessment method was applied to nominal wake measurement tests of a very large crude oil carrier model ship. The nominal wake measurement results were compared with existing experimental database by other measurement methods, with its assessed uncertainty.

1. Introduction

The flow field around a ship's hull is a very important issue in improving its hydrodynamic performance; however, it is highly complex due to flow characteristics, that is, turbulence, Three-Dimensional (3D) separation, and free-surface effects. Because of difficulties in direct measurements of a flow field around a full-scale ship, flow field measurements and analysis around a hull have mainly been attempted in laboratory scale models. For example, wake flow measurement results of a scaled model have been used for practical ship and propeller design.

For provision of flow field measurement results, test uncertainty of experiments must be assessed and given with test results. Longo and Stern (2005) suggested a method for investigating test uncertainty associated with towing tank tests and applied it to assess uncertainty of a flow measurement test using Pitot tubes for a surface combatant model. Kume et al. (2006) investigated flow field around Very Large Crude oil Carrier (VLCC) model and provided the results with the test uncertainty. The International Towing Tank Conference (ITTC) (ITTC, 2008a) provides a practical guidance to assess test uncertainty of conventional flow and force measurements in a towing tank.

In recent years, a non-intrusive optical technique such as particle image velocimetry (PIV) has been applied to flow measurements in towing tanks and replacing conventional Pitot tube measurements of which test procedure and uncertainty assessment are well established, as stated above. Gui et al. (2001a, 2001b) applied the window masking technique to a Two-Dimensional (2D) PIV system in a towing tank for measuring a wake field behind a surface-piercing plate. They also reconstructed Three-Dimensional (3D) wake structure by stacking 2D flow measurement results for a surface combatant without a propeller. The window masking technique was made possible to reduce systematic errors on the mean velocity and Reynolds stress measurement. Seo et al. (2016a) carried out 2D PIV measurements of the wake behind a VLCC model in self-propulsion conditions.

The Stereoscopic PIV (SPIV), which employs two cameras to get a planar velocity field with Three-Component (3C) velocity vectors, has been introduced to towing tank tests: wake flow measurements behind a propeller (Anschau and Mach, 2007; Seo et al.,

* Corresponding author.
E-mail address: thamjang@snu.ac.kr (J. Seo).
Peer review under responsibility of Society of Naval Architects of Korea.

https://doi.org/10.1016/j.ijnaoe.2017.11.005

Nomenclature

b	Systematic standard uncertainty [-]
D	Dynamic range [-]
Fr	Froude number based on L_{PP} and U_{input} [-]
k	Turbulence kinetic energy $\left(\frac{1}{2}(\overline{u'u'}+\overline{v'v'}+\overline{w'w'})\right)$ [m^2/s^2]
L_{PP}	Length between perpendiculars [m]
N	Number of data samples [-]
R	Radius of the propeller model [m]
Re	Reynolds number based on L_{PP} and U_{input} [-]
s	Random standard uncertainty [-]
T	Thickness of the laser sheet [m]
Δt	Time interval between laser pulses [μs]
U_{95}	Expanded uncertainty with 95% confidence level [-]
U_{beacon}	Beacon-measured towing carriage speed [m/s]
U_{input}	Towing carriage speed input [m/s]
U_{wheel}	Wheel encoder-measured towing carriage speed [m/s]
u, v, w	Velocities in (x, y, z) directions [m/s]
$\overline{u}, \overline{v}, \overline{w}$	Ensemble-averaged velocities in (x, y, z) directions [m/s]
$\overline{u'u'}, \overline{v'v'}, \overline{w'w'}$	Reynolds normal stresses in (x, y, z) directions [m^2/s^2]
$\overline{u'v'}, \overline{u'w'}, \overline{v'w'}$	Reynolds shear stresses [m^2/s^2]
x, y, z	Cartesian coordinates in the physical coordinate system [m]

2016b), a tidal stream turbine (Seo et al., 2016c), and a model ship in captive dynamic maneuvering tests (Yoon et al., 2015). Although SPIV is now a relatively mature measurement technique, its practical applications in a towing tank are still in a development phase, thus a test uncertainty assessment procedure for towing tank tests is in demand.

Uncertainty of convectional PIV with Two-Components (2C) has been investigated in many studies (Raffel et al., 1998; ITTC, 2008b; Nobach and Bodenschatz, 2009; Timmins et al., 2012; Sciacchitano et al., 2013; Wilson and Smith, 2013). It is known that a significant portion of the overall uncertainty of PIV systems comes from cross-correlation and sub-pixel estimation algorithms. However, test uncertainty of a PIV system in the towing tank can be more sensitive to certain environmental conditions than analysis algorithms (Seol et al., 2013). The environmental factors include flow-induced vibration of submerged optical instruments, large distortion of images due to limitations of optical arrangements, and limited number of images acquired during a towing carriage run.

Measuring a low-turbulence uniform flow is an effective approach to estimate the systematic uncertainty of PIV systems for use in a towing tank. Grizzi et al. (2010) suggested a novel calibration approach based on uniform flow measurements. Their flow-based method does not require the target plate for spatial calibration of the SPIV system, thus eliminating errors derived from the calibration target misalignment. By uniform flow measurements, Yoon et al. (2015) carried out systematic uncertainty assessment of atowed underwater SPIV system.

In this paper, we present a test uncertainty assessment method of a SPIV system in a towing tank, focusing on nominal wake measurement. This paper was intended as a comparable reference for researchers or experimenters who are carrying out SPIV measurements in a towing tank. A SPIV system was installed to the towing tank of Seoul National University (SNU) and its test uncertainty was assessed based on the procedure of ITTC (2008b) and Yoon et al. (2015). The test uncertainty assessment method was applied to nominal wake measurement for a VLCC model and the results and uncertainty are compared with existing experimental data obtained by different experimental methods.

This paper is organized as follows. Section 2 shows principles of test uncertainty assessment for nominal wake measurement tests. Details of the experimental setup are followed in Section 3. Section 4 and 5 explain results of uniform flow and nominal wake measurements, respectively. The summary and conclusions of this work are presented in Section 6.

2. Test uncertainty assessment procedure

In SPIV tests, instantaneous velocity vectors (u, v, w) are acquired during a carriage run and ensemble-averaged. The ensemble-averaged velocity vectors ($\overline{u}, \overline{v}, \overline{w}$) are presented as test results. The expanded uncertainty of the ensemble-averaged velocity, i.e., $U_{\overline{u},95}$, $U_{\overline{v},95}$, and $U_{\overline{w},95}$, should be assessed.

The expanded standard uncertainty with 95% confidence level is calculated from systematic and random standard uncertainty (ASME, 2005). Data reduction equations of ($\overline{u}, \overline{v}, \overline{w}$) in SPIV measurement are quite complicate, therefore it is hard to identify each elemental error source and assess elemental systematic standard uncertainty, which are required for deriving $b_{\overline{u}}$, $b_{\overline{v}}$, and $b_{\overline{w}}$. In this study, instead of elemental systematic standard uncertainty and uncertainty propagation, uniform flow measurement was repeated to get a measurement population mean for comparison with independent measurements. Random standard uncertainty, $s_{\overline{u}}$, $s_{\overline{v}}$, and $s_{\overline{w}}$ could be evaluated by obtaining the standard deviation of repeated nominal wake measurement with large number of carriage runs.

SPIV measurements provide planar velocity field and the test uncertainty is not homogeneous on the plane. It is reported that test error increases near the edge of the field of view, while the center region shows less error (Seol et al., 2013). A test uncertainty value should consider spatial variation. In this study, a representative standard uncertainty that contains 95% of local standard uncertainty on a measurement plane was defined from the spatial mean and spatial root-mean-square (RMS) of assessed local test uncertainty by assuming Student's distribution, as follows.

$$(\text{Representative standard uncertainty}) = \sqrt{(\text{Spatial mean})^2 + 2 \times (\text{Spatial RMS})^2}$$

Uncertainty propagation in non-dimensionalization procedure is also considered in this study. Once an ensemble-averaged flow field is obtained, physical properties of length and velocity dimensions are non-dimensionalized by R and U_{beacon}, respectively.

In addition, Reynolds stresses are derived from instantaneous velocity field measurement results and presented as dimensionless values, after being divided by U^2_{beacon}. The expanded uncertainty of Reynolds stresses is also assessed in this study.

3. Experimental set-up

3.1. Towing tank

Experimental measurements were conducted in the towing tank, which is 110 m long, 8 m wide, and 3.5 m deep. A schematic drawing of the towing tank is shown in Fig. 1. The towing carriage for speeds from 0.100 to 5.000 m/s is driven by four servo-motors, and its speed is controlled by a closed loop feedback system.

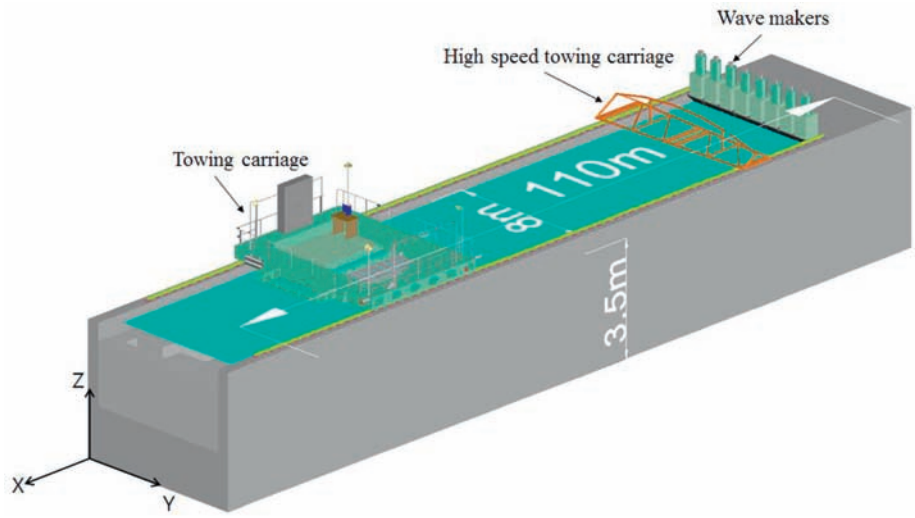

Fig. 1. A schematic drawing of the towing tank of SNU.

To assess the SPIV test uncertainty, the uncertainty of the flow speed condition should be estimated first. For comparing with the uniform flow measured by the towed underwater SPIV, two independent speed measurement devices were used: an optical sensor and rotary encoder system.

For optical measurement, three beacons with 15 m spacing were placed on the carriage rail and the time to pass beacons was measured with the temporal resolution of 100 Hz by an optical sensor. The rotary encoder measured rotational speed of the towing carriage wheel. The circumference of the carriage wheel was 2.000 m, and its revolution was counted by the 10-bit signal with the sampling rate of 100 Hz.

Tables 1 and 2 show expanded uncertainties of the towing carriage speed measured by the optical sensor and wheel encoder, respectively. The carriage speed measurement was repeated 30 times to ensure that the number of samples is large enough. The expanded uncertainty of the optical method was lower than that of the rotary encoder, thus the optical measurement results were used as the reference of the towing carriage speed.

3.2. Stereoscopic PIV system

The underwater SPIV system, which contains an Nd:YAG pulse laser and two digital cameras, was designed and manufactured by LaVision GmbH (Göttingen, Germany). Fig. 2 shows a schematic drawing of the SPIV setup for wake measurements. Two digital cameras with lenses and a scheimpflug angle controller were located in each vertical waterproof cylinder to capture the particle images from two different views. The focal length of the cameras was 50 mm. The cameras were capable of capturing a monochrome image with 4096 (12-bit) brightness levels. The repetition rate of the cameras was 14.4 Hz, meaning that 7.2 image pairs could be taken per one second.

To illuminate the field of view, a pulsed laser sheet with 2 mm of thickness and polyamide tracer particles with the mean diameter of 18 μm were used. The laser pulse power was 200 mJ for each laser beam. In this work, polyamide particles, water, and surfactant were mixed in a pre-mixer tank and then the mixture was discharged into towing tank water by pressurized air. For each day of the experiment, 1 kg of tracer particles was seeded into the towing tank, especially along the path of the test model. The particle density on a particle image was typically over 0.05 particles per a pixel.

Fig. 3 shows the optical arrangement of the laser sheet and two digital cameras. In this optical setup, the field of view size was 120 mm × 120 mm. The right-handed Cartesian coordinate system was used; positive *x*, *y* and *z* denotes the downstream, starboard and upward directions, respectively. The SPIV measurement plane for uniform flow and nominal wake test was *yz* plane, which was perpendicular to the propeller axis.

Two planar velocity fields were obtained by each camera first. Captured particle images by the cameras were analyzed with Davis Version 8.1 of LaVision GmbH; a multi-pass cross-correlation was applied with three-time iterations on an interrogation window of 128 × 128 pixels without overlap and two-time iterations on 64 × 64 pixels with a 50% overlap. A moving average filter was applied to the 2D velocity fields during multi-pass cross-correlation steps.

Two resultant instantaneous 2D2C velocity fields from different cameras were combined to derive a 2D3C velocity field, using calibration results. A two-leveled calibration plate with grooved lines was used for the 3D calibration (Calluaud and David, 2004). Fig. 4 shows images of the calibration target taken by two cameras. White dots with the diameter of 5 mm were arranged on a black calibration plate. Grooved lines on the target plate has the depth of 3 mm and spacing of 15 mm. The locations of the dots in the physical coordinate and on the camera images were matched by using third-order polynomial equations.

Table 1
Uncertainties of the beacon-measured carriage speed (U_{beacon}).

Speed input [m/s]	U_{input}	0.500	1.000	1.500
Beacon-measured speed [m/s]	U_{beacon}	0.4945	0.9959	1.4978
Systematic standard uncertainty [$\%U_{beacon}$]	$b_{U_{beacon}}$	0.0327	0.0663	0.0997
Random standard uncertainty [$\%U_{beacon}$]	$s_{U_{beacon}}$	0.491	0.385	0.277
Expanded uncertainty [$\%U_{beacon}$]	$U_{U_{beacon},95}$	0.984	0.781	0.589

Table 2
Uncertainties of the wheel encoder-measured carriage speed (U_{wheel}).

Speed input [m/s]	U_{input}	0.500	1.000	1.500
Encoder-measured speed [m/s]	U_{wheel}	500.9	1001.7	1502.8
Systematic standard uncertainty [$\%U_{wheel}$]	$b_{U_{wheel}}$	1.28	0.583	0.347
Random standard uncertainty [$\%U_{wheel}$]	$s_{U_{wheel}}$	1.02	0.497	0.208
Expanded uncertainty [$\%U_{wheel}$]	$U_{U_{wheel},95}$	3.28	1.53	0.81

Fig. 2. A schematic drawing of the SPIV setup for wake measurements.

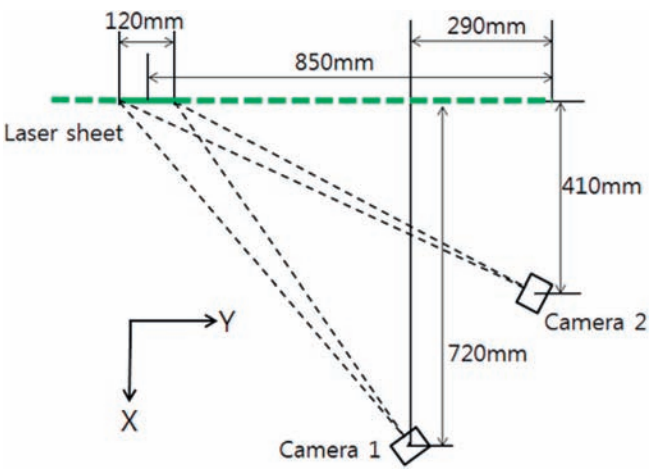

Fig. 3. Optical arrangement of a laser sheet and two cameras.

Acquired 3C velocity field had deformation. It was corrected to the physical coordinate system with the calibration. Images by Camera 2, which suffered greater distortion, showed large error in image dewarping than that by Camera 1. On the resultant 2D3C velocity field, the distance between velocity vectors was 1.5 mm.

Spurious vectors with unrealistic magnitude were filtered with a given threshold; velocity vectors of which magnitude was over 110% of U_{input} were deleted. It was decided after examining the time-history of measured instantaneous velocity fields, in which the magnitude of instantaneous velocity vectors hardly exceeded the threshold. As the nominal wake measurement dealt with retarded flow behind the ship model, turbulence intensity was concentrated where the flow speed was low. Therefore high instantaneous velocity was hardly possible, and the threshold was considered reasonable.

Validated instantaneous velocity vector fields were then ensemble-averaged. Because of the repetition rate of the SPIV system, the sampling rate of SPIV measurement was fixed as 7.2 Hz. The number of samples or carriage runs was varied in this study to find an optimal number.

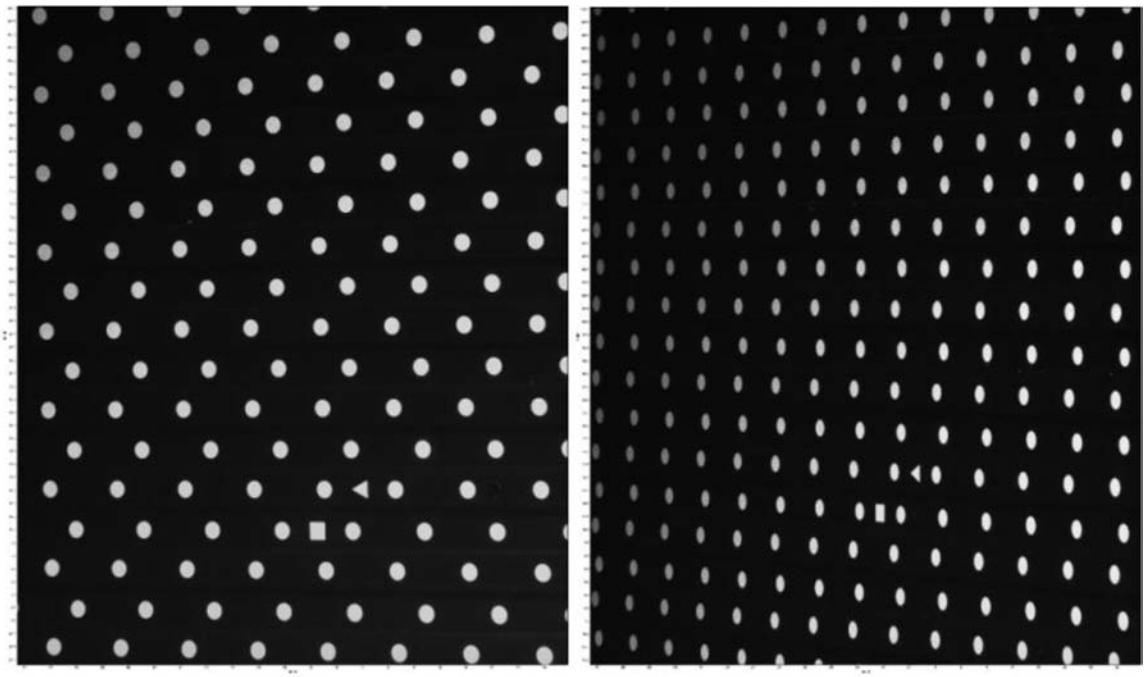

Fig. 4. Images of the calibration plate taken with Camera 1 (left) and Camera 2 (right).

3.3. LDV system

A single-component underwater LDV system was used to measure $\overline{u}$ and $\overline{u'u'}$. The LDV system was designed and manufactured by Dantec Dynamics A/S (Skovlunde, Denmark). It comprised a continuous air-cooled 300 mW Argon laser (Stellar-Pro-L Multi-Line/300, manufactured by Modu-laser, Centerville, UT), a beam transmitter, 60 × 24 fiber manipulators, 60 × 61 FlowLite waterproof LDV probe, back-scatter receiving optics, and FFT analyzer (manufactured by Dantec Dynamics A/S). The spacing and diameter of laser beams with a wavelength of 514 nm (green) were 38.0 mm and 1.35 mm, respectively. A circular convex lens with a focal length of 399.5 mm was used to converge two beams at a single point. All LDV measurements were controlled by BSA Flow Software Version 5.20 (Dantec Dynamics A/S). In this study, the data acquisition rate ranged from 10 to 50 Hz, because of the flow and seeding conditions.

3.4. Test model

A 1/100 scaled model of a VLCC (Kim et al., 2001) was used for nominal wake field measurement. The test model is here referred to as KVLCC2. Fig. 5 shows the body plan and profiles of KVLCC2, and principal particulars of the ship in full scale and model are presented in Table 3.

The ship model was painted with matte black paint to decrease reflection of laser light on the model surface. To initiate turbulent flow, two vertical arrays of studs were attached at the bow: one at the middle of the bulbous bow and another at 5% of L_{PP} from the fore perpendicular. For more detailed information, refer to the ITTC recommendations (ITTC, 2011).

Wake distribution behind a hull without a propeller at the design speed was measured. The measurement plane was at the propeller plane location, 98.25% of L_{PP} from the forward perpendicular. The design speed was 15.5 knots at the full scale. The corresponding Froude number and model speed were 0.142 and 0.797 m/s, respectively. The ship model was fixed at the even keel attitude during the tests, as previous studies on nominal wake measurement (Kim et al., 2001; Lee et al., 2003).

4. Uniform flow measurement

4.1. Time intervals between laser pulses variations

Uniform flow measurements with the SPIV system were first carried out at the towing speed of 1.000 m/s, which represents the towing speed range commonly used for model tests in the towing tank. In the towing speed condition, Δt was varied to control the particle displacement in the longitudinal direction between two laser pulses, Δx, and identify the effects of $\Delta x/T$ on the uniform flow measurement results.

Fig. 6 shows the spatial mean and RMS of ensemble-averaged velocity from 300 data samples, which could be acquired during a single carriage run. The cases of short tracer particle displacement, i.e., $\Delta x = 50$ and 100 μm, displayed a noticeable difference from the other cases with larger particle displacements. The corresponding particle displacements on the particle image was under one pixel and the error from sub-pixel analysis, approximately 0.1 pixel (Raffel et al., 1998), became dominant. In larger particle displacement cases, however, the error from sub-pixel analysis was constant. Consequently the weight of the error from sub-pixel analysis reduced.

As Δt and Δx increased, the number of tracer particles which exist on both particle image frames reduced, while the error from cross-correlation was expected to increase. At the case of 800 μm displacement, however, the mean and standard deviation of the velocity components were similar with other cases where Δx was over 100 μm. It seems that the particle density on particle images were high enough to keep suitable number of particles for cross-correlation analysis, and moving average filtering worked well even in the cases where out-of-plane loss of cross correlation was around 40% (Adrian and Westerweel, 2011).

We concluded that Δx of 350 μm, i.e., the particle displacement of four pixels and $\Delta x/T$ of 17.5%, was adequate for flow

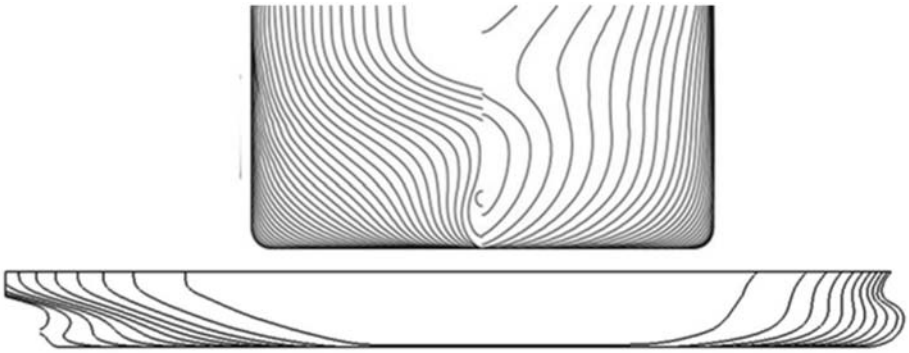

Fig. 5. Body plan and profiles of KVLCC2.

Table 3
Principal particulars of KVLCC2.

	Full scale	Model scale
Scale ratio [-]	1	1/100
Length between perpendiculars[m]	320.0	3.20
Breadth [m]	58.0	0.58
Draft [m]	20.8	0.208
Block coefficient [-]	0.8098	
Propeller radius [m]	4.9	0.049

measurement. As the nominal wake was a retarded flow and u ranges from zero at the propeller hub to U_{input} at far field, half of U_{input} was set as the representative longitudinal velocity of the nominal wake field and Δt was derived from it, instead of U_{input}. For nominal wake measurement of the KVLCC2 model at the design speed, 0.797 m/s, Δt of 878 μs could be used.

The spatial RMS presented in Fig. 6 is considered as the spatial variability. Note that the spatial variability of w is much smaller than those of u and v. As pointed out by Yoon et al. (2015), the differences are accounted for by the optical arrangement of the SPIV system. It is explained in the systematic standard uncertainty section in detail.

5. Towing speed variations

The SPIV measurements were also carried out at three different towing speeds (0.500, 1.000, and 1.500 m/s) to investigate the effect of free-surface waves and flows around the SPIV system. As the SPIV system consists of blunt circular cylinders, strong free-surface waves and vortex shedding are developed in high towing speed cases, which may affect the flow field at the measurement plane and/or cause vortex-induced vibration.

In this measurement, the time intervals for U_{input} of 0.500, 1.000, 1.500 m/s were set to 700, 350, and 233 μs respectively, thus the displacement of tracer particles between particle image frames were kept constant, 350 μm or four pixels, as described above.

Table 4 shows the spatial arithmetic mean and RMS of the ensemble-averaged velocity components measured at the three speeds. All the differences were approximately 1% of U_{input}, and effects of flow speed variation seems to be insignificant. One noteworthiness was that the error of $\overline{u}$ increased in high speed condition., while the error of $\overline{v}$ decreased. As two velocity components were strongly coupled to each other, the portion changed, although the magnitude of the total error was preserved.

5.1. Systematic uncertainty in uniform flow measurements

For a reference case, uniform flow measurements were carried out at U_{input} of 1000 mm/s and Δt of 350 μs Measurements were repeated over 30 times with waiting time of 20 min between carriage runs. By preliminary tests, it was confirmed that initial turbulence eddies larger than the SPIV's spatial resolution were dissipated within the waiting time and the initial turbulence effects were negligible.

Fig. 7 shows distributions of the systematic standard uncertainty of time-averaged velocity measurements. The systematic standard uncertainties, $b_{\overline{u}}$ and $b_{\overline{v}}$, were less than 2% of U_{beacon}, and their distributions were very similar. $b_{\overline{w}}$ had relatively small magnitude compared with both $b_{\overline{u}}$ and $b_{\overline{v}}$, and its distribution also differed from the others.

The angle between the camera sight and laser sheet of the present towed underwater SPIV system was 26° and generally smaller than in ordinary SPIV systems because of the limited space for optical components arrangement. As $\overline{u}$ and $\overline{v}$ were derived mainly from the transverse particle displacement on the particle images, the camera arrangement could affect the systematic errors of both $\overline{u}$ and $\overline{v}$. In the case of $\overline{w}$, however, it was mainly derived from the vertical displacement of tracer particles on the image, where the distortion of the field of view was small, and had small systematic error.

Fig. 8 shows systematic standard uncertainties of Reynolds normal stress, which are normalized by U^2_{beacon}. Similar to the systematic standard uncertainties of the ensemble-averaged velocity components, $b_{\overline{u'u'}}$ and $b_{\overline{v'v'}}$ were larger than $b_{\overline{w'w'}}$. Table 5 summaries the systematic standard uncertainties of ensemble-averaged velocity components and Reynolds stresses.

Also, we carried out measurement of $\overline{u}$ by using the LDV with the same method with the SPIV case. In the LDV measurements, $b_{\overline{u}}$ and $b_{\overline{u'u'}}$ were 0.35% of U_{beacon} and 0.232% of U^2_{beacon}, respectively. Compared with the LDV measurement, $b_{\overline{u}}$ from the SPIV measurement was relatively large, whereas $b_{\overline{u'u'}}$ was much smaller. It is thought that velocity fluctuation by small-scale eddies of initial turbulence cannot be captured by the SPIV system and showed small systematic standard uncertainty.

6. Nominal wake measurement

Fig. 9 shows the probability density function for u measured with the SPIV and LDV systems. The measurement location was $(y/R, z/R) = (0.6, -0.6)$, where the velocity gradient was stiff. By SPIV and LDV measurements, $\overline{u}$, $\overline{v}$, and $\overline{w}$ obtained from 300 data samples per a carriage run. The carriage run was repeated over 30 times to achieve large sample size (ASME, 2005). As the number of data samples and carriage runs increased, the probability density function converged and the results of two independent measurements did not produce a statistically significant difference between SPIV

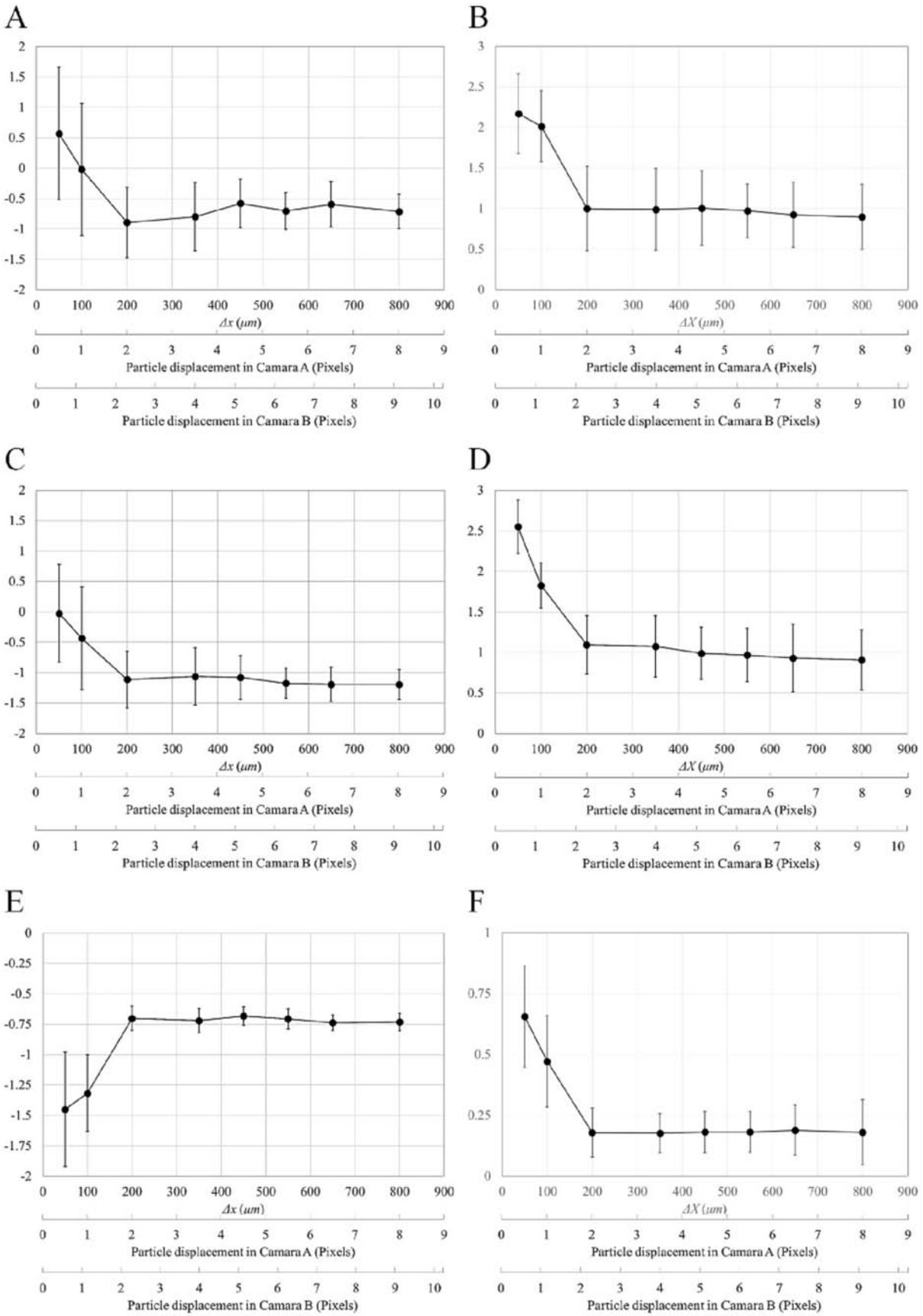

Fig. 6. Variation of the ensemble-averaged velocity and Reynolds normal stress with particle displacement variation (dot: spatial mean, error bar: spatial RMS; A: $\overline{u} - U_{beacon}$ $[\%U_{beacon}]$, B: $\overline{u'u'}/U_{beacon}^2 \times 10^4$, C: $\overline{v}$ $[\%U_{beacon}]$, D: $\overline{v'v'}/U_{beacon}^2 \times 10^4$, E: $\overline{w}$ $[\%U_{beacon}]$, F: $\overline{w'w'}/U_{beacon}^2 \times 10^4$).

Table 4
Spatial mean and RMS of the time-averaged velocity components.

	Spatial mean			Spatial RMS		
U_{input} [m/s]	0.500	1.000	1.500	0.500	1.000	1.500
U_{beacon} [m/s]	0.4945	0.9959	1.4978	0.4945	0.9959	1.4978
$\overline{u} - U_{beacon}$ [$\%U_{beacon}$]	−0.69	−0.90	−1.13	0.77	0.91	0.94
$\overline{v}$ [$\%U_{beacon}$]	−1.14	−1.05	−0.98	0.48	0.59	0.65
$\overline{w}$ [$\%U_{beacon}$]	−0.92	−0.84	−0.75	0.13	0.12	0.13

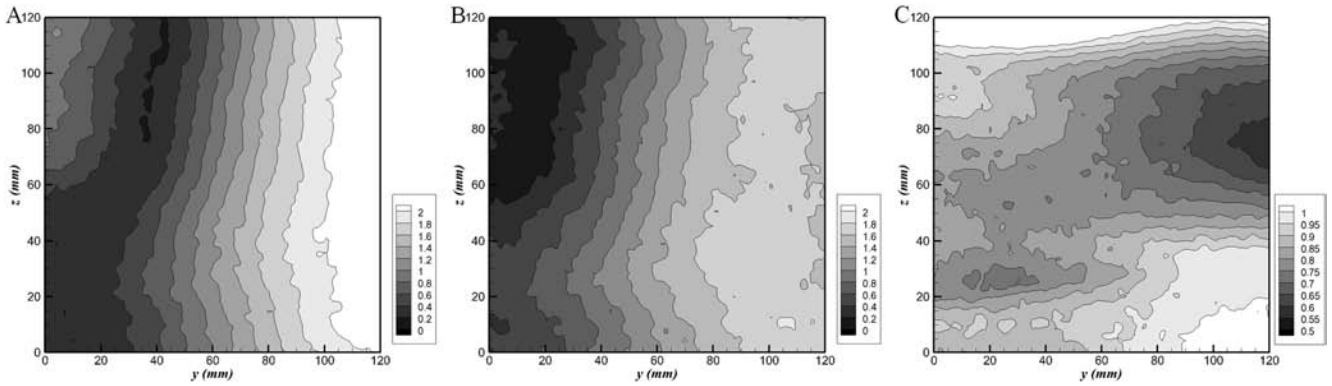

Fig. 7. The systematic standard uncertainty of the mean velocity measurement (A: $b_{\overline{u}}$ [$\%U_{beacon}$], B: $b_{\overline{v}}$ [$\%U_{beacon}$], C: $b_{\overline{w}}$ [$\%U_{beacon}$].

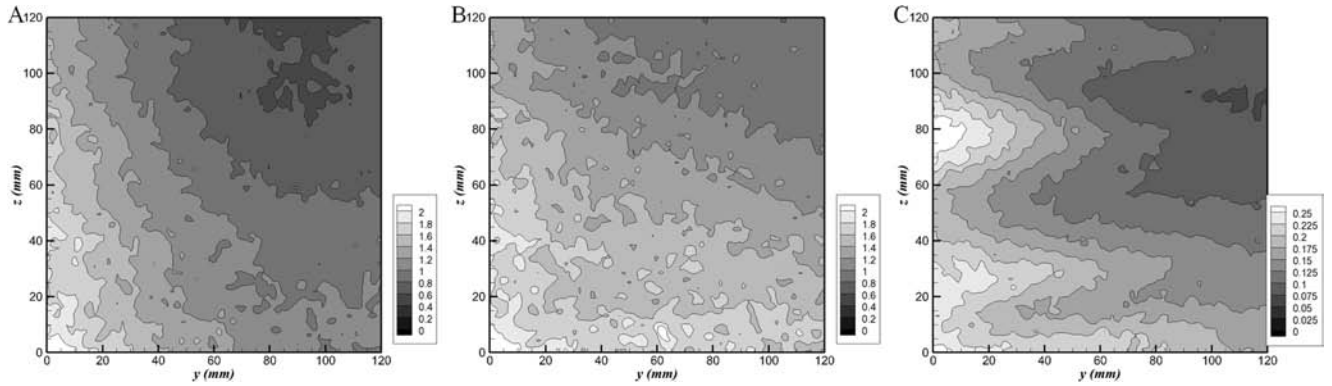

Fig. 8. The systematic standard uncertainty of the Reynolds normal stress measurement (A: $b_{\overline{u'u'}}/U^2_{beacon} \times 10^4$, B: $b_{\overline{v'v'}}/U^2_{beacon} \times 10^4$, C: $b_{\overline{w'w'}}/U^2_{beacon} \times 10^4$).

and LDV measurements. For both of SPIV and LDV, N of 10000 appeared to be large enough to obtain an accurate and representative results.

Fig. 10 shows changes of $s_{\overline{u}}$ and $s_{\overline{u'u'}}$ of SPIV and LDV measurements, according to the number of repeated carriage runs. Uncertainties of SPIV wake measurement on KVLCC2 during single carriage run are summarized in Table 6. Systematic standard uncertainties in Table 6 were obtained from the uniform flow measurements (see Table 5). All random standard uncertainties except for $S_{\overline{w}}$ are larger than systematic standard uncertainties.

Table 5
Systematic standard uncertainties of uniform flow measurements.

	Spatial mean	Spatial RMS	Representative standard uncertainty
$b_{\overline{u}}$ [$\%U_{beacon}$]	1.10	0.68	1.75
$b_{\overline{v}}$ [$\%U_{beacon}$]	1.07	0.56	1.54
$b_{\overline{w}}$ [$\%U_{beacon}$]	0.84	0.12	0.87
$b_{\overline{u'u'}}$ [$\%U^2_{beacon}$]	1.02×10^{-2}	0.51×10^{-2}	1.44×10^{-2}
$b_{\overline{v'v'}}$ [$\%U^2_{beacon}$]	1.16×10^{-2}	0.38×10^{-2}	1.38×10^{-2}
$b_{\overline{w'w'}}$ [$\%U^2_{beacon}$]	0.18×10^{-2}	0.05×10^{-2}	0.21×10^{-2}
$b_{\overline{u'v'}}$ [$\%U^2_{beacon}$]	0.42×10^{-2}	0.19×10^{-2}	0.57×10^{-2}
$b_{\overline{u'w'}}$ [$\%U^2_{beacon}$]	0.11×10^{-2}	0.04×10^{-2}	0.14×10^{-2}
$b_{\overline{v'w'}}$ [$\%U^2_{beacon}$]	0.10×10^{-2}	0.04×10^{-2}	0.13×10^{-2}
b_k [$\%U^2_{beacon}$]	1.19×10^{-2}	0.52×10^{-2}	1.58×10^{-2}

Fig. 11 shows the nominal wake field of KVLCC2 measured by the SPIV system. The origin of the coordinate system was set at the center of the propeller shaft. So-called hook-shaped velocity contours due to longitudinal bilge vortex were well captured by the SPIV measurement. This is a well-known characteristic of the wake field (for detailed information, refer to Kim et al. (2001) and Lee et al. (2003)).

In Fig. 12, nominal wake fields measured with the SPIV and LDV systems are compared with other existing results in the literature; measurements in a towing tank with five-hole Pitot tubes (Kim

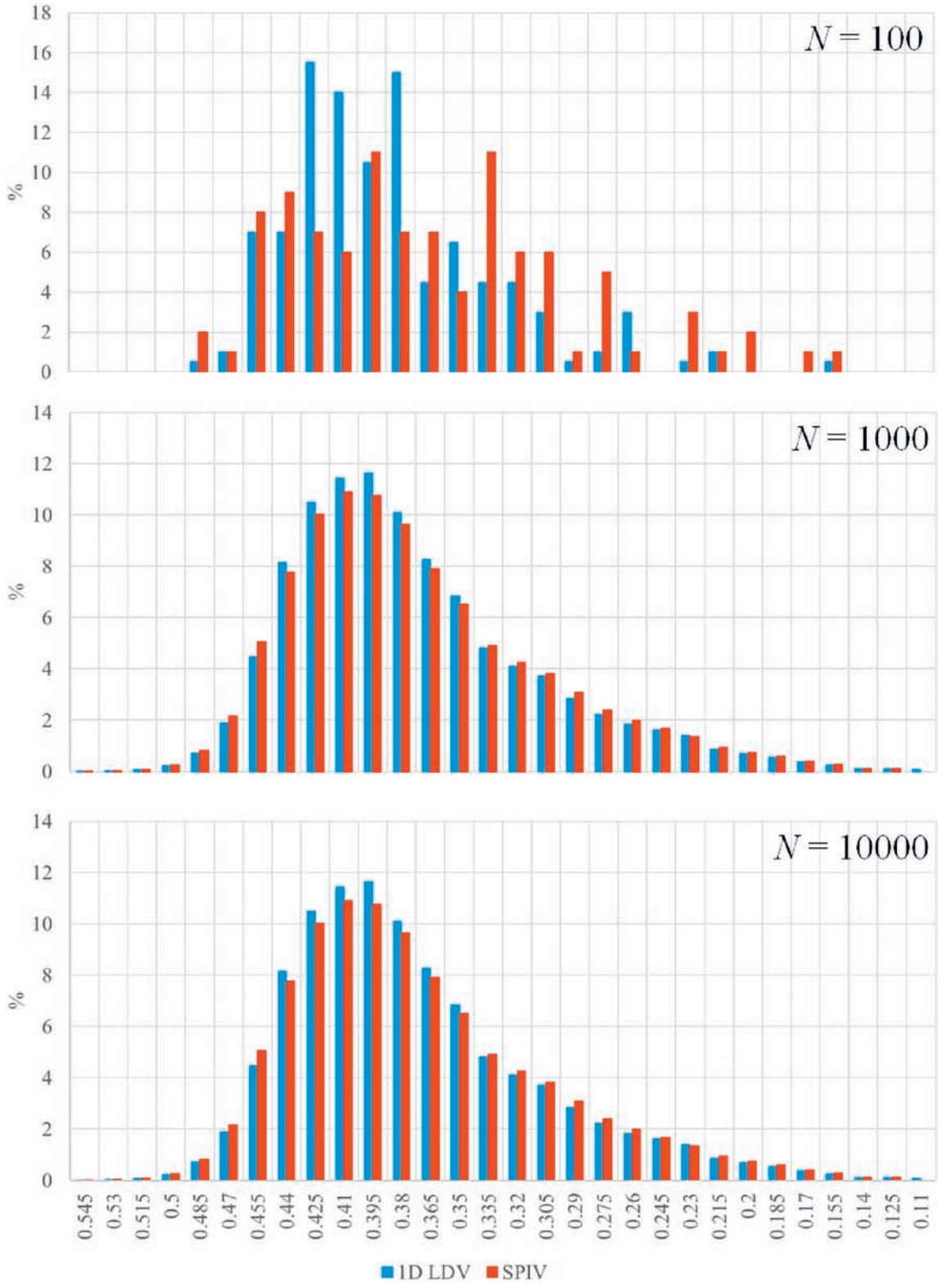

Fig. 9. Probability density distribution of u at $y/R = 0.6$ and $z/R = -0.6$, according to the number of data samples (N).

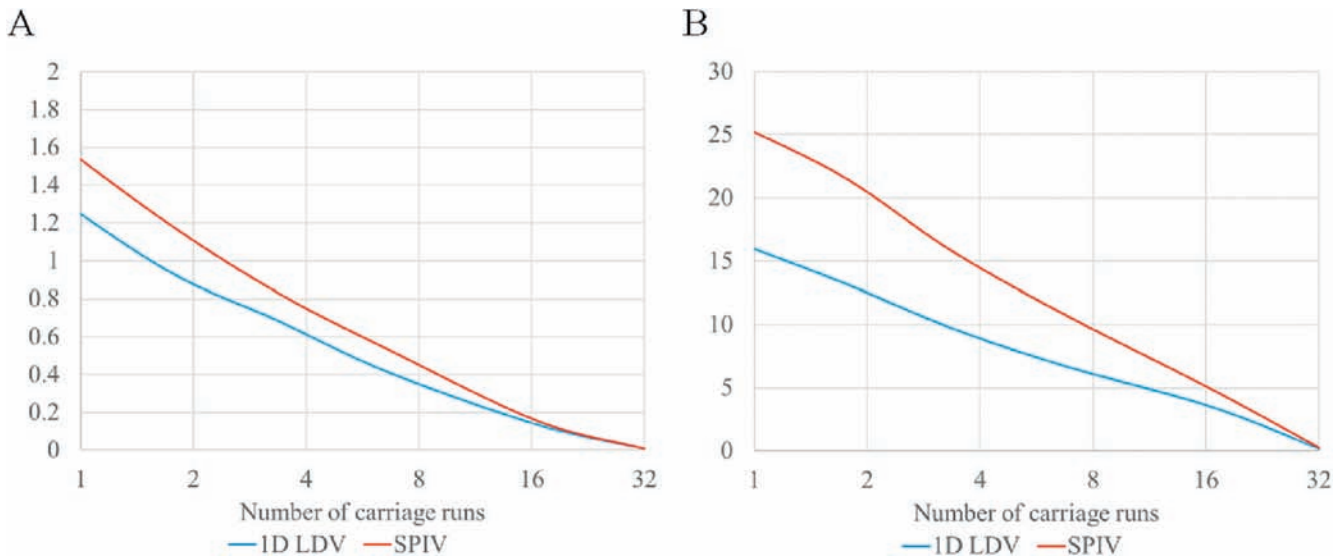

Fig. 10. Changes of $s_{\overline{u}}$ [$\%U_{beacon}$] (A) and $s_{\overline{u'u'}}/U^2_{beacon} \times 10^4$ (B), according to the number of carriage runs.

Table 6
Uncertainties of the nominal wake measurement by the SPIV system.

	Systematic standard uncertainties	Random standard uncertainties	Expanded uncertainty with 95% confidence level
$\overline{u}$ [$\%U_{beacon}$]	1.75	1.63	4.78
$\overline{v}$ [$\%U_{beacon}$]	1.54	0.73	3.42
$\overline{w}$ [$\%U_{beacon}$]	0.87	0.42	1.94
$\overline{u'u'}$ [$\%U^2_{beacon}$]	1.44×10^{-2}	26.1×10^{-2}	52.3×10^{-2}
$\overline{v'v'}$ [$\%U^2_{beacon}$]	1.38×10^{-2}	18.7×10^{-2}	37.5×10^{-2}
$\overline{w'w'}$ [$\%U^2_{beacon}$]	0.21×10^{-2}	11.2×10^{-2}	22.4×10^{-2}
$\overline{u'v'}$ [$\%U^2_{beacon}$]	0.57×10^{-2}	3.14×10^{-2}	6.38×10^{-2}
$\overline{u'w'}$ [$\%U^2_{beacon}$]	0.14×10^{-2}	5.31×10^{-2}	10.6×10^{-2}
$\overline{v'w'}$ [$\%U^2_{beacon}$]	0.13×10^{-2}	2.47×10^{-2}	4.95×10^{-2}
k [$\%U^2_{beacon}$]	1.58×10^{-2}	22.4×10^{-2}	44.9×10^{-2}

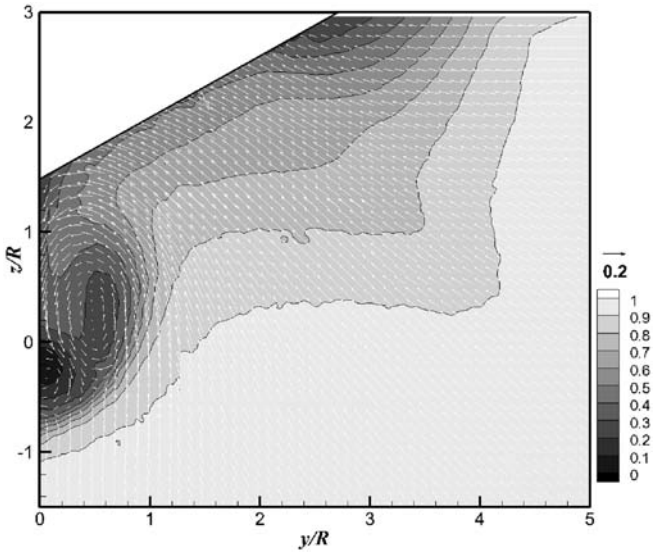

Fig. 11. $\overline{u}/U_{input}$ contours and cross-flow vectors at the propeller plane of KVLCC2.

et al., 2001), measurements in a wind tunnel with hotwire anemometers (Lee et al., 2003), measurements in a towing tank with 2C-2D PIV and a 1D Pitot-static tube (Seo et al., 2016a). The measurements with the five-hole Pitot tubes and the hotwire anemometer were carried out at a *Re* of 4.6×10^6, while the others at a *Re* of 2.3×10^6. The Reynolds number effect such as wake contraction was not observable.

Fig. 13 shows $\overline{u'u'}$ distributions measured with four different measuring techniques. All contour maps followed a similar pattern of $\overline{u'u'}$ distribution whereas significant difference in local maxima among the different methods. The discrepancy possibly resulted from differences in flow and model conditions and temporal and spatial resolutions. Relatively high surface roughness due to matte black paint appeared to yield a significant increase of local maxima of $\overline{u'u'}$.

In general, the hotwire anemometer results with smooth model surface showed lower turbulence intensity. In low *Re* condition tests, however, matte black paint, which caused high surface roughness was used to the model and it may have increased the local turbulence intensity. In addition, SPIV showed larger local maxima than other measurement results, as the spatial resolution of SPIV was inferior to that of other methods in the same *Re* condition.

Table 7 shows a comparison of the expanded uncertainties of nominal wake measurements for KVLCC2. The expanded uncertainty denotes the combined uncertainty multiplied by a coverage factor of 2 for a 95% confidence interval and the combined uncertainty means the RMS of the systematic standard uncertainty and the random standard uncertainty (for detailed information, see

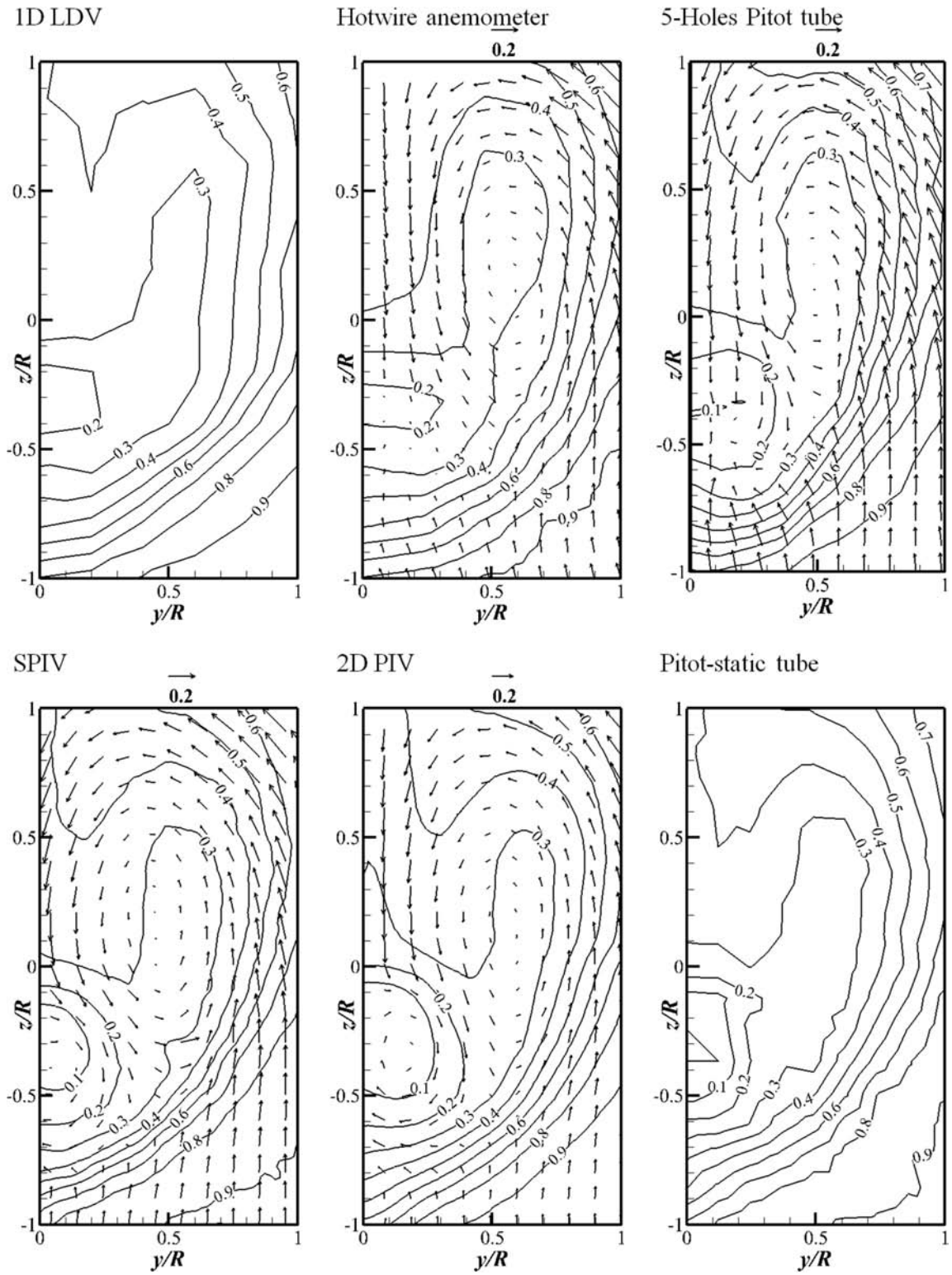

Fig. 12. Nominal wake fields for KVLCC2 measured with different measuring methods (Contour lines denote $\overline{u}$ and the vectors denote tangential velocity components.).

ASME (2005)). For comparison, the expanded uncertainties with a 95% confidence interval were expressed as percentages of D for each physical property.

Relatively large uncertainty of SPIV measurement can be accounted for the optical setup and inferior spatial resolution (which causes an increase in systematic uncertainty) and a smaller number of data samples (which causes an increase in random uncertainty). In addition, the model surface treatment could also affect the test uncertainty, especially for turbulence measurement.

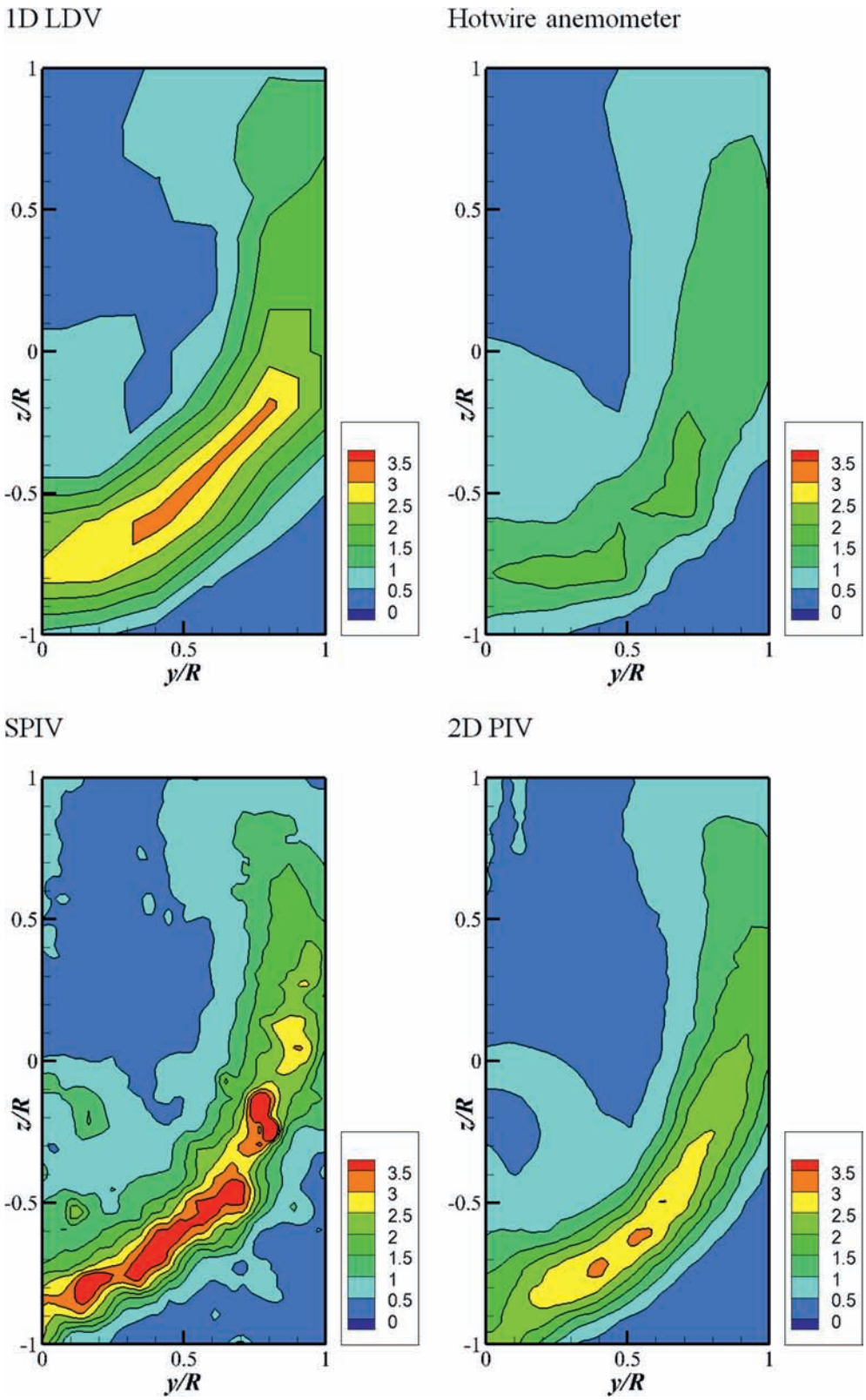

Fig. 13. Contours of $\overline{u'u'}/U_{input}^2 \times 10^4$ at the propeller plane of KVLCC2.

7. Concluding remarks

In this work, we carried out uniform flow and nominal wake measurements for KVLCC2 with the SPIV system. The quality of the SPIV measurements was quantitatively assessed through experimental uncertainty analysis which is based on the methods of ITTC (2008b) and Yoon et al. (2015).

For a reference case, uniform flow was measured to estimate the

Table 7
Expanded uncertainties of nominal wake measurement for KVLCC2.

	Spatial resolution [%R]	$\overline{u}$ [%$D_{\overline{u}}$]	$\overline{v}$ [%$D_{\overline{v}}$]	$\overline{w}$ [%$D_{\overline{w}}$]	$\overline{u'u'}$ [%$D_{\overline{u'u'}}$]	k [%D_k]
Hotwire anemometer (Lee et al., 2003)	2.9	0.5	0.7	1.0	7.8	12.8
Five-hole Pitot tube (Kim et al., 2001)	0.95	0.82	1.78	1.60	–	–
2C-2D PIV (Seo et al., 2016a, b, c)	2.1	1.21	4.28	3.85	4.32	13.9
Pitot-static tube (Seo et al., 2016a, b, c)	4.1	0.51	–	–	–	–
LDV (present)	1.5	1.21	–	–	15.1	–
SPIV (present)	6.1	4.15	5.23	3.70	14.7	14.0

systematic standard uncertainty of mean velocity and turbulence properties. By the uniform flow measurement, it was found that errors in the x and y directional components of the velocity and turbulence properties were larger than those of the z directional components, due to the optical arrangement of the towed underwater SPIV system.

In addition, uniform flow measurement results for different test conditions were conducted to investigate the effects of flow around the SPIV system and particle displacement on the SPIV results. Effects of blockage of the camera cylinder were examined, but there were no significant changes in measured mean velocity field with towing speed variations. In the particle displacement variation case, the magnitude of the error was consistent when the particle displacement was over one pixel.

The random standard uncertainty of KVLCC2 wake measurements during a single carriage run was assessed and compared with previous experimental results. For mean velocity field, the results showed good agreement, while SPIV results showed large local maxima of Reynolds normal stress, due to spatial resolution and test uncertainty.

Acknowledgement

This research was supported by the Ministry of Defense (Civil Military Technology Center), the IT R&D program of MOTIE/KEIT (Grant No. 100660329), the National Research Foundation of Korea (Grant No. 2016R1D1A1A09917670), and National Research Council of Science & Technology (CMP-16-03-KISTI), grant by the Korea government.

References

Adrian, R.J., Westerweel, J., 2011. Particle Image Velocimetry. Cambridge University Press, New York, NY.
Anschau, P., Mach, K.P., 2007. Application of a stereo PIV system for investigations of flow fields in towing tank and cavitation tunnel. Arch. Civ. Mech. Eng. 7 (3), 5–17.
American Society of Mechanical Engineers, 2005. Test Uncertainty. The American Society of Mechanical Engineers Performance Test Code, 19.1.
Calluaud, D., David, L., 2004. Stereoscopic particle image velocimetry measurements of the flow around a surface-mounted block. Exp. Fluids 36 (1), 53–61.
Grizzi, S., Pereira, F., Di Felice, F., 2010. A simplified, flow-based calibration method for stereoscopic PIV. Exp. Fluids 48 (3), 473–486.
Gui, L., Longo, J., Stern, F., 2001a. Biases of PIV measurement of turbulent flow and the masked correlation-based interrogation algorithm. Exp. Fluids 30 (1), 27–35.
Gui, L., Longo, J., Stern, F., 2001b. Towing tank PIV measurement system, data, and uncertainty assessment for DTMB model 5512. Exp. Fluids 31 (3), 336–346.
International Towing Tank Conference, 2008a. Guide to the expression of uncertainty in experimental hydrodynamics. In: International Towing Tank Conference Recommended Procedures and Guidelines, 7.5-02-01-01.
International Towing Tank Conference, 2008b. Uncertainty analysis: particle image velocimetry. In: International Towing Tank Conference Recommended Procedures and Guidelines, 7.5-02-01-01.
International Towing Tank Conference, 2011. Recommended procedures and guidelines: ship models. In: International Towing Tank Conference Recommended Procedures and Guidelines, 7.5-01-01-01.
Kim, W.J., Van, S.H., Kim, D.H., 2001. Measurement of flows around modern commercial ship models. Exp. Fluids 31 (5), 567–578.
Kume, K., Hasegawa, J., Tsukada, Y., Fujisawa, J., Fukasawa, R., Hinatsu, M., 2006. Measurements of hydrodynamic forces, surface pressure, and wake for obliquely towed tanker model and uncertainty analysis for CFD validation. J. Mar. Sci. Technol. 11 (2), 65–75.
Lee, S.J., Kim, H.R., Kim, W.J., Van, S.H., 2003. Wind tunnel tests on flow characteristics of the KRISO 3,600 TEU Containership and 300K VLCC double-deck ship models. J. Ship Res. 47 (1), 24–38.
Longo, J., Stern, F., 2005. Uncertainty assessment for towing tank tests with example for surface combatant DTMB model 5415. J. Ship Res. 49 (1), 55–68.
Nobach, H., Bodenschatz, E., 2009. Limitations of accuracy in PIV due to individual variations of particle image intensities. Exp. Fluids 47 (1), 27–38.
Raffel, M., Willert, C.E., Kompenhans, J., 1998. Particle Image Velocimetry: a Practical Guide. Springer, Berlin, Germany.
Sciacchitano, A., Wieneke, B., Scarano, F., 2013. PIV uncertainty quantification by image matching. Meas. Sci. Technol. 24 (4), 045302.
Seo, J., Seol, D.M., Han, B., Rhee, S.H., 2016a. Turbulent wake field reconstruction of VLCC models using two-dimensional towed underwater PIV measurements. Ocean. Eng. 118, 28–40.
Seo, J., Lee, S.J., Han, B., Rhee, S.H., 2016b. Influence of design parameter variations for propeller-boss-cap-fins on hub vortex reduction. J. Ship Res. 60 (4), 1–16.
Seo, J., Lee, S.J., Choi, W.-S., Park, S.T., Rhee, S.H., 2016c. Experimental study on kinetic energy conversion of horizontal axis tidal stream turbine. Renew. Energy 97, 784–797.
Seol, D.M., Seo, J., Rhee, S.H., 2013. Towed underwater PIV measurement for free-surface effects on turbulent wake of a surface-piercing body. Int. J. Nav. Archit. Ocean Eng. 5 (3), 404–413.
Timmins, B.H., Wilson, B.W., Smith, B.L., Vlachos, P.P., 2012. A method for automatic estimation of instantaneous local uncertainty in particle image velocimetry measurements. Exp. Fluids 53 (4), 1133–1147.
Wilson, B.M., Smith, B.L., 2013. Uncertainty on PIV mean and fluctuating velocity due to bias and random errors. Meas. Sci. Technol. 24 (3), 035302.
Yoon, H., Longo, J., Toda, Y., Stern, F., 2015. Benchmark CFD validation data for surface combatant 5415 in PMM maneuvers – Part II: phase-averaged stereoscopic PIV flow field measurements. Ocean. Eng. 109, 735–750.